Doppler-Shifted Cyclotron Resonance of Helicon Waves in Single-Crystal Aluminum*

JOHN L. STANFORD† AND EDWARD A. STERN‡
Department of Physics and Astronomy, University of Maryland, College Park, Maryland
(Received 22 November 1965)

Results are presented of measurements of Doppler-shifted cyclotron resonance (DSCR) of helicon waves in single-crystal aluminum with the magnetic field and helicon propagation along the [100] and [110] directions. The Gaussian radius of curvature of the Fermi surface in the second zone is measured at the point where the surface normal is along [100]. The experimental value for the radius of curvature is 0.99 ± 0.03 times the free-electron value, in agreement with the expected value. For [110], it is shown that DSCR absorption edges at an elliptic limiting point on an arm of the third-zone Fermi-surface "monster," and on finite orbits involving a large fraction of the electrons on the second-zone surface, are expected to occur almost simultaneously. The difficulties associated with interpretation of the data when finite-orbit absorption edges exist are discussed. It is shown that beyond an estimate of the [110] curvature, which is in surprisingly good agreement with the calculated value, a more precise interpretation of the [110] data cannot be justified. The merits of the helicon DSCR method for Fermi-surface studies are discussed, and it is concluded that in general useful information can be obtained only on very pure samples with $\omega_c\tau\gtrsim100$, where ω_c is the cyclotron frequency and τ the conduction-electron relaxation time.

I. INTRODUCTION

WHEN a magnetic field is applied to solids at low temperatures such that $\omega_c\tau\gg1$, where ω_c is the cyclotron frequency and τ the relaxation time of the conduction electrons, the solid becomes transparent to a class of electromagnetic waves (magnetoplasma oscillations) called helicons. Recently, these helicons have been utilized to obtain information about the electronic structure of solids. Ever since their prediction in 1960,[1] and their discovery in 1961,[2] helicon waves have been the subject of numerous investigations, both experimental and theoretical.[3]

The first use of the Doppler-shifted cyclotron resonance (DSCR) of helicon waves was proposed by Stern,[4] who showed that information about the Fermi surface at single points should be obtainable for relatively simple surfaces. Investigators have obtained information about the Fermi wave number in polycrystalline samples of sodium, potassium, and indium.[5] The purpose of this paper is to present the first detailed results of DSCR helicon studies in single-crystal aluminum along the [100] and [110] directions.

The local and nonlocal helicon theory is briefly presented in Sec. II. Section III contains a discussion of the experimental apparatus and sample preparation. The experiment results are presented in Sec. IV, and an interpretation of the single-crystal-aluminum data is given in Sec. V. Some conclusions concerning the general applicability of the DSCR-helicon method to Fermi-surface studies is given in the final section, VI.

II. HELICON THEORY

A. Local Regime

For pure metals and high magnetic fields such that $\omega_c\tau\gg1$, an electromagnetic "window" is opened up for the propagation through metals of circularly polarized electromagnetic waves (helicons) having the sense of polarization of the cyclotron rotation of the metallic conduction carriers. In the "local" regime, where the helicon wave number q and electronic mean free path l satisfy the condition $ql\ll1$, the helicon propagates for all frequencies below ω_c and the helicon dispersion relation for infinite $\omega_c\tau$ is

$$q^2=\frac{\omega\mu_0 ne}{B}. \tag{1}$$

Here ω is the helicon frequency, n is the number of carriers per cubic meter, μ_0 is the magnetic permeability of free space, e is the electronic charge and B is the applied static magnetic field. In a real metal with magnetoresistance and finite τ, the helicon amplitude is decreased by e^{-1} in a distance of u/π wavelengths, where $u=R_HB/\rho(B)$. R_H is the Hall constant and $\rho(B)$ is the resistivity of the metal in the field B. For a free-electron gas, where $\rho(B)=\rho(0)$, $u=\omega_c\tau$. If the magnetoresistivity of the metal is appreciable, the helicons are more heavily attenuated, having a damping length inversely proportional to the total resistivity of the metal.

---

* Submitted in partial fulfillment of the requirements for the Ph.D. degree in the Department of Physics and Astronomy of the University of Maryland. Supported in part by the Advanced Research Projects Agency under contract No. SD-101.

† NSF Cooperative Fellow 1961–65. Present address: Institute for Atomic Research and Department of Physics, Iowa State University, Ames, Iowa.

‡ On leave of absence 1965–66: Temporary address: Department of Physics, University of Washington, Seattle, Washington.

[1] P. Aigrain, *Proceedings of the International Conference on Semiconductor Physics, Prague, 1960* (Publishing House of the Czechoslovak Academy of Sciences, Prague, 1961), p. 224. Also see O. V. Konstantinov and V. I. Perel, Zh. Eksperim. i Teor. Fiz. **38**, 161 (1960) [English transl.: Soviet Phys.—JETP **11**, 117 (1960)].

[2] R. Bowers, C. R. Legendy, and F. E. Rose, Phys. Rev. Letters **7**, 339 (1961).

[3] For a list of references, see S. J. Buchsbaum and R. Bowers, in *Proceedings of the Symposium on Plasma Effects in Solids, Paris, 1964*, edited by J. Bok (Academic Press Inc., New York, 1965).

[4] E. A. Stern, Phys. Rev. Letters **10**, 91 (1963). The same method was proposed for ultrasonic shear waves by T. Kjeldaas, Jr., Phys. Rev. **113**, 1473 (1959).

[5] M. T. Taylor, Phys. Rev. **137**, A1145 (1965).

In the local limit, the propagation "window" is for all $\omega<\omega_c$, but nonlocal effects become important as the frequency is increased. The upper frequency limit of the transmission window is lowered by these nonlocal effects, which will now be discussed.

B. Nonlocal Regime (DSCR Theory)

The attenuation of helicon waves with frequencies $\omega<\omega_c$ is small in the local regime ($ql\ll 1$), provided the metal is sufficiently pure and the magnetic field sufficiently strong that $\omega_c\tau\gg 1$. As the wavelength of the helicon wave is decreased, however, the nonlocal region ($ql\gtrsim 1$) is entered, and a critical wavelength is reached, below which the helicon wave attenuation is extremely strong, even in the limit of $\omega_c\tau\to\infty$. It is just this property which permits the use of helicons in obtaining information about the Fermi surface.[4]

The physical reason for this nonlocal attenuation is a Doppler-shifted mechanism. A given band of electrons on the Fermi surface has an average velocity $\bar{v}_B$ along the direction of the field B. If the helicon wave number q is along B, the electrons do not see an electromagnetic disturbance of frequency ω set up by the helicon, but a Doppler-shifted frequency[6]

$$\omega'=\omega+q\bar{v}_B. \tag{2}$$

If ω' happens to coincide with the electron cyclotron frequency ω_c, absorption of energy out of the helicon wave by the conduction electrons will occur. This phenomenon is called Doppler-shifted cyclotron resonance.[7] From a consideration of v_B averaged around an orbit, it can be shown that the DSCR absorption condition is[8]

$$B/q=(\hbar/2\pi e)\partial A/\partial k_B, \tag{3}$$

where A is the area enclosed by the cyclotron orbit and k_B is the electronic wave number along B. Other groups of electrons on the Fermi surface can also contribute to the absorption process, and in fact, an absorption edge will be reached when the last group of electrons which satisfy (3) are in resonance. The absorption edge (Kjeldaas edge) can be seen to occur whenever the absolute value of (3) is a maximum. Experimentally, it is generally easier to fix ω and sweep B. In this case, the DSCR absorption occurs for B lower than the absorption edge field B_E, while for $B>B_E$ no group of carriers is able to undergo DSCR. For a spherical Fermi surface, the last group of electrons in DSCR are those able to do the most Doppler shifting of the helicon frequency; that is, those having $\bar{v}_B=v_F$, the Fermi velocity. Thus, the DSCR edge occurs on the "point" orbit whose normal is along B. For a general elliptic limiting point, the DSCR edge condition is

$$B_E/q_E=(\hbar/e)(\rho_1\rho_2)^{1/2}, \tag{4}$$

where $\rho_1\rho_2$ is the product of the two principal radii of curvature of the Fermi surface at the point whose surface normal is along the field B. The product $\rho_1\rho_2$ is called the Gaussian radius of curvature of the surface. For a spherical surface, $\rho_1=\rho_2=k_F$, the Fermi wave number. Thus, for relatively simple surfaces the curvature may be obtained point-by-point, providing B_E and q_E can be measured.

It may happen that the surface has its greatest value of $|\partial A/\partial k_B|$ not at a point orbit, but on a finite orbit. For example, $|\partial A/\partial k_B|$ has a maximum value for the inflection-point orbit of a Fermi-surface "neck," when the field is along the neck direction.[9] It has been shown that the possibility of absorption edges occurring on finite orbits can add considerable complication to DSCR data evaluation.[10]

For convenience, we summarize here the results of Ref. 10 pertinent to our discussion:

(1) For Fermi surfaces having axial symmetry about the magnetic field direction, $\mathrm{Im}\sigma(q)$ is found to have a delta-function dependence at the Kjeldaas edge for a finite-orbit case in the limit of $\omega_c\tau\to\infty$. Here $\sigma(q)$ is the nonlocal, wave-number-dependent helicon conductivity function. An infinity does not occur in $\mathrm{Im}\sigma(q_E)$ for a point-orbit edge.

(2) Because of the infinity in $\mathrm{Im}\sigma(q_E)$ for the finite orbit case, the helicon dispersion relation is double-valued, e.g., two wave numbers exist for a single frequency. q is double-valued for all ω for infinite $\omega_c\tau$, but only for a limited region for finite $\omega_c\tau$. The point-orbit case also exhibits a double-valued behavior, but only over a small range of ω even for $\omega_c\tau\to\infty$.

(3) The peak in the resistive part R of the sample surface impedance occurs at q_m and B_m, where the ω versus q^2 curve has a maximum and the helicon group velocity is zero ($\partial\omega/\partial q=0$). This does not coincide with the Kjeldaas-edge wave number q_E.

For a spherical Fermi surface and infinite $\omega_c\tau$, a fixed-frequency experiment will yield a measured edge field B_m about $\frac{1}{2}\%$ lower than the Kjeldaas edge B_E. This difference is generally within experimental error. For finite-orbit edges, on the other hand, the difference can be appreciable. For the finite-orbit model chosen (the spin-density wave Fermi surface predicted for potassium by Overhauser[11]), q_m is 14% lower than q_E. Since the difference q_E-q_m can only be calculated if the details of the Fermi-surface topology are known, care must be exercised in interpreting DSCR data obtained by the surface-impedance method.

[6] Equation (2) is true strictly speaking only in the limit of $\omega_c\tau\to\infty$, so that the helicon has a uniquely defined wave number q. For finite $\omega_c\tau$, the problem must be solved self-consistently. See Ref. 10.

[7] P. B. Miller and R. R. Haering, Phys. Rev. **128**, 126 (1962). J. Kirsch, *ibid.* **133**, A1390 (1964).

[8] Reference 4. The relation between $\bar{v}_B$ and $\partial A/\partial k_B$ is given by W. A. Harrison, Phys. Rev. **118**, 1190 (1960).

[9] A. B. Pippard, *The Dynamics of Conduction Electrons* (Gordon and Breach Science Publishers, Inc., New York, 1965), p. 129.

[10] J. C. McGroddy, J. L. Stanford, and E. A. Stern, Phys. Rev. **141**, 437 (1966). J. C. McGroddy and J. L. Stanford, Bull. Am. Phys. Soc. **10**, 384 (1965).

[11] A. W. Overhauser, Phys. Rev. Letters **13**, 190 (1964).

(4) Finite values of $\omega_c\tau$ cause the position of the surface resistance peak to be shifted to higher fields for fixed frequencies.

(5) The reactive part X of the surface impedance also has structure which does not exactly coincide with the peak in R for finite $\omega_c\tau$. Since it is not generally possible to isolate either R or X experimentally, the structures in R and X occurring at different fields make it difficult to precisely determine B_m unless $\omega_c\tau$ is extremely high. For $\omega_c\tau \gtrsim 100$, the structures should be sufficiently sharp to allow the experimental edge field B_m to be unambiguously specified.

In conclusion, sample surface-impedance measurements are difficult to interpret unless $\omega_c\tau$ is quite high, and even then, for the case of a finite-orbit edge, the measured quantities do not have a simple relationship to the Fermi-surface topology. Precise information about Fermi surfaces with finite-orbit edges can be obtained, however, if $\omega_c\tau$ is high enough to allow measurement of q_E by the interference fringe method discussed in the next section. A value of $\omega_c\tau \gtrsim 100$ should allow measurement of both q_m and q_E, the latter being directly related to the Fermi-surface curvature.

III. EXPERIMENTAL PROCEDURES

A. Apparatus

The experimental apparatus is similar to that used first by Grimes and Buchsbaum.[12] A large, static field B is applied perpendicular to the large face of a thin plate sample. Helicons are excited on one side of the sample by rf currents in an exciter coil, and propagate through the sample to the other side where they are detected by a receiver coil. The exciter and receiver coils are adjusted to be mutually perpendicular to minimize direct coupling around the sample. A small directly coupled signal is still permitted to be induced in the receiver coil, however. It is approximately independent of magnetic field and one to two orders of magnitude larger than the helicon signal. The pickup voltage V_{RF} is thus the sum of the two signals. A complete elimination of the directly coupled signal is not desired since it aids in identification of the helicon signal, as will now be seen. Recall that the helicon wavelength is a function of the magnetic field B [Eq. (1) gives the relation in the local limit]. When B is changed such that the number of helicon half-wavelengths in the sample thickness has changed from N to $N\pm1$, where N is an integer, the pickup voltage V_{RF} changes from a maximum to a neighboring minimum, or vice versa, producing an interference fringe pattern such as the experimental curve of Fig. 1.

As the field is brought down from a high value, $B>B_E$, the fringe amplitudes decrease due to a combination of more sample attenuation ($\omega_c\tau$ decreasing with decreasing B) and the changing transmission coefficient of the sample (because σ, and thus the dielectric constant ϵ, is a function of B). Below the absorption edge field B_E, the helicon is highly attenuated, with amplitudes generally damping to e^{-1} in less than a wavelength. From Fig. 1 it is not obvious just where B_E occurs, and hence a method for determining the edge field was sought. Two such methods were found. One is discussed later in Sec. IV. In the vicinity of the edge, the sample is in the process of changing from being transparent to being opaque to the rf electromagnetic radiation. That is, for $B>B_E$ there is transmission, while for $B<B_E$ the rf is not allowed to propagate through the sample. The sample dielectric constant is thus undergoing a drastic change near B_E and it would not be surprising if the impedance of the rf coils near the sample experienced a corresponding change. With greater sensitivity, such a change is in fact found, and occurs in the form of an inflection point in the receiver output.[5] Because of the spherical Fermi surface of sodium, B_E can be calculated for a given helicon frequency.[5] We find it to lie on the inflection point to within experimental accuracy.

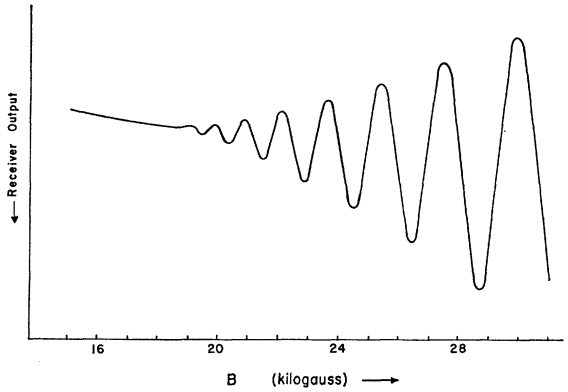

FIG. 1. Tracing of direct transmission helicon fringes in Na (R.R.R.~6500) for 3 Mc/sec and 4.2°K. Sample thickness: 0.74 mm.

The use of a modulation of the magnetic field together with a phase-sensitive detector here would be beneficial, since the edge could be more accurately determined. Not only would there be an enhancement of the signal-to-noise ratio, but the inflection in V_{RF} would appear as a maximum or minimum in the output of the phase-sensitive detector (because of the inherent differentiation of the signal with respect to B which occurs with this technique), which can be more accurately located than an inflection point. The phase-sensitive detection apparatus is shown in Fig. 2. The superconducting solenoid power supply is modulated by a 5 cps reference signal, causing the magnetic field to have a 5 cps component of a few hundred gauss peak-to-peak, superimposed on the static field B.

The magnetic field of the superconducting solenoid is known to an accuracy of $\pm2\%$, and was calibrated by

[12] C. C. Grimes and S. J. Buchsbaum, Phys. Rev. Letters 12, 357 (1964).

utilizing the low-frequency standing-wave helicon resonance[13] in a sodium plate. The solenoid is not compensated, and has field inhomogeneities on the order of 1% within the working volume.

The helicon frequency was measured to better than 0.1% with a BC-221 frequency meter for the sodium work, and to better than one part in 10^4 on an electronic counter in the aluminum work.

B. Sample Preparation

(*i*) *Sodium*

The experiment was initiated using sodium metal for the following reasons:

(1) sodium has a relatively low magnetoresistivity,
(2) high-purity sodium was available,
(3) the Fermi surface of sodium is thought to be very nearly spherical, so that theoretical and experimental results can be easily compared.

The high-purity sodium metal was graciously given to us by C. E. Taylor of the Lawrence Radiation Laboratory, Livermore, California. Checking the residual resistance ratio (R.R.R.) by the method of Bean, DeBlois, and Nesbitt,[14] we obtained a value of R.R.R. $\sim$6500 for this material. This high purity yields $\omega_c\tau\sim 40$ in 10 kG, and together with its relatively low magnetoresistivity, is sufficient to allow easy helicon propagation.

The specimens used were in the form of polycrystalline plates, approximately $1\times 10\times 10$ mm^3 in size. The metal is pressed into the shape of a slab of required thickness between two glass microscope slides, being kept continuously under dry mineral oil to reduce oxidation of the surface.

(*ii*) *Aluminum*

The aluminum was Cominco grade 69 material, obtained in the form of ingots. A sample spark-cut from the ingot showed a residual resistance ratio $\sim$7000 by the Bean, DeBlois, and Nesbitt method. The value of $\omega_c\tau$, estimated from the decay of low-frequency helicons in this material, is on the order of 15 for 10 kG.

Single crystals in the [100] and [110] directions were prepared by the following procedure: Single crystals were selected from the Cominco ingots, x-ray oriented, and samples were spark-cut to minimize sample strain. The samples were on the order of $1\times 10\times 10$ mm^3. In order to obtain appreciable helicon fringe heights, the samples have to be flat and parallel to much better than a helicon wavelength in the sample. For 100 kc/sec and 10 kG, $\lambda\sim 5\times 10^{-3}$ cm in aluminum.

The [110] crystal was chemically handlapped and electropolished with the following technique[15] to insure parallelness of the two sides and to minimize "rounding off" in the polishing process. A Lucite block has a cylindrical hole drilled through it perpendicular to one face. A right-circular cylindrical aluminum piston is machined to slide snugly in the cylindrical hole. The sample slab is now cemented onto one end of the piston, making electrical contact with it. A piece of Teflon cloth is fastened over an ordinary aluminum plate. The sample can now be moved across the Teflon cloth, riding up and down on its guide piston as the sample becomes polished.

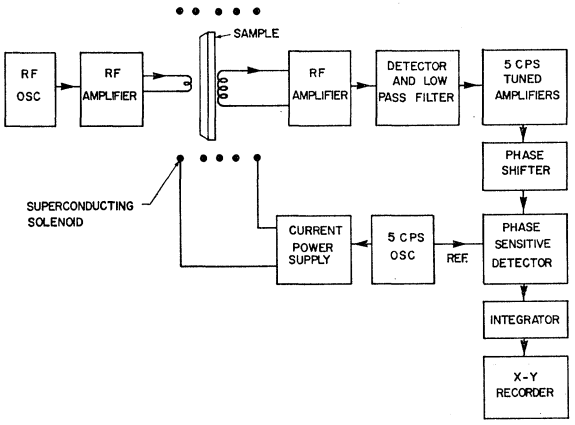

FIG. 2. Block diagram of helicon DSCR experiment with phase-sensitive detection.

For chemical handlapping, a medium concentration of H_2O and $CuCl_2$ is poured on the Teflon cloth. For electropolishing, a 50% ethyl alcohol, 40% H_3PO_4 and 10% glycerine (by volume) solution is used. The piston and the Teflon-covered plate become the two electropolishing electrodes across which the electropolishing potential is applied.

It was later discovered that the [110] axis was not quite normal to the sample ($\sim 2°$ off). However, the experimental data shows no difference within experimental error whether B was along [110] or the normal to the sample. The [110] crystal was $1.13\pm 1\%$ mm thick at room temperature. The other two dimensions were approximately 9 mm$\times$14 mm. A thermal contraction correction of 0.4% between room temperature and 4°K used by Chambers and Jones[16] was also applied here, for both the [110] and [100] crystals.

The [100] crystal was found to be sufficiently smooth to see large fringes without electropolishing, so that it was only chemically handlapped. The final surface roughness, seen under a microscope, was estimated to be about 2×10^{-4} cm. The [100] axis was aligned along the sample normal to within 1°. Its average thickness at room temperature was $0.40\pm 1\%$ mm, while its other dimensions were about 8 mm$\times$10 mm.

[13] J. R. Houck and R. Bowers, Rev. Sci. Instr. **35**, 1170 (1964).
[14] C. P. Bean, R. W. DeBlois, and L. B. Nesbitt, J. Appl. Phys. **30**, 1976 (1959).
[15] We are indebted to Professor J. F. Koch for showing us this method.
[16] R. G. Chambers and B. K. Jones, Proc. Roy. Soc. (London) **A270**, 417 (1962).

IV. EXPERIMENTAL RESULTS

A. Sodium

An experimental curve for sodium using phase-sensitive detection and an rf frequency of 3 Mc/sec is shown in Fig. 3. The experimental value for the edge is

$$17.5\pm0.3\text{ kG}. \tag{5}$$

Despite the fact that sodium suffers a partial martensitic phase transformation from a bcc to a hcp structure below about 30°K, any distortions of the Fermi surface will remain unobservable by the helicon DSCR technique, which measures only the largest Fermi surface curvature for a given direction of magnetic field. Since the two phases coexist, the large curvature of the spherical Fermi surface in the bcc phase will be the first absorption edge reached. The helicon wave ceases to exist below B_E because of the extremely heavy attenuation encountered inside the edge, and thus no lower edges will be observed by the helicon DSCR method.

For a spherical Fermi surface it is possible to calculate B_E for a given ω. Using a lattice constant[17] of 4.225Å and one electron per atom, one obtains for $\omega/2\pi=3$ Mc/sec,

$$B_E=17.7\text{ kG}. \tag{6}$$

As discussed in Sec. II, a more detailed analysis reveals that the measured edge will occur about $\frac{1}{2}\%$ below B_E. Hence, the expected value for $\omega_c\tau\rightarrow\infty$ is 17.6 kG, agreeing favorably with the experimental value (5). This is expected since the Fermi surface of sodium is thought to be very nearly spherical, and $\omega_c\tau\sim45$ for our sodium at this field. Similar results confirming the spherical surface of sodium have been obtained by Taylor[5] using a different technique (the surface-impedance method) with helicon DSCR.

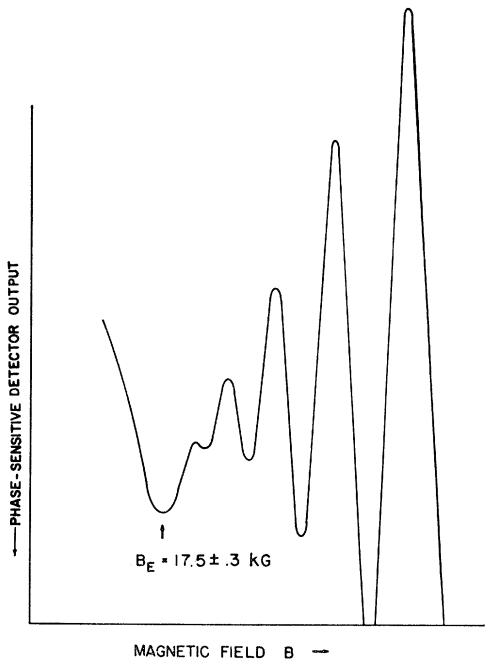

FIG. 3. Tracing of helicon fringe derivative curve obtained with phase-sensitive detection apparatus for Na metal at 3 Mc/sec and 4.2°K. Sample thickness: 0.58 mm.

[17] C. S. Barrett, Acta Cryst. **9**, 671 (1956).

With the surface-impedance technique, B and ω may be determined, but not the helicon wavenumber q. The value of q is then calculated from the known dispersion relation connecting ω and q for a spherical Fermi surface. However, the calculation is complicated for nonspherical Fermi surfaces, and in fact, has been published for only one other case, that of cylindrical symmetry.[18] Since the Fermi-surface curvature is related to B_E and q_E, and not B_E and ω_E, the beauty of the surface impedance technique is marred by difficulties of interpretation for more complicated Fermi surfaces.

In contrast, the interference fringe technique allows a direct measurement of q and thus in principle this method can be extended to any general Fermi-surface shape. Figure 4 shows an experimental (interference method) and theoretical plot of q^2 versus B^{-1} for 3 Mc/sec in sodium. In the local regime ($\omega_c\gg qv_F$), Eq. (1) shows that q^2 is proportional to B^{-1} for fixed ω. As B is increased, nonlocal behavior occurs as the absorption edge is approached, and q^2 deviates from its simple B^{-1} dependence. Both of these regions are displayed in Fig. 4. It can be shown that

$$\frac{q^2}{q^2_{\text{local}}}=\frac{\text{Im}\sigma(q,B)}{\text{Im}\sigma(0,B)}, \tag{7}$$

where $\sigma(q,B)$ is the nonlocal helicon conductivity function. For a spherical Fermi surface and $\omega_c\tau\rightarrow\infty$,

$$\frac{\text{Im}\sigma(q,B)}{\text{Im}\sigma(0,B)}=f\left(\frac{q}{B}\right), \tag{8}$$

where the function f has been given by various investigators.[19] We have solved Eq. (7) self-consistently by numerical means to obtain the theoretical nonlocal q^2 dependence on B^{-1} as shown by the solid line in Fig. 4. The agreement with experiment is seen to be good. The small region of double-valuedness in q^2 for given B near the edge, discussed in Sec. II, is also shown on the theoretical curve. At the wave number q_m, the peak in the surface resistance occurs[10] (infinite slope on the q^2 versus B^{-1} graph). It is here that the helicon has zero group velocity, and can enter into strong resonance with the exciting fields at the sample surface.

B. Aluminum

Representative experimental curves for both the [100] and the [110] single-crystal aluminum samples

[18] Reference 10. Also, see S. Rodriguez and A. W. Overhauser, Phys. Rev. **141**, 431 (1966).

[19] See, for example, Refs. 7 and 10 and J. J. Quinn and S. Rodriguez, Phys. Rev. **133**, A1590 (1964).

are shown in Figs. 5 and 6. The scale and zero is not the same for all the curves, and the fringe amplitudes are generally on the order of millivolts on the xy-recorder graphs, after amplification of 10^2 to 10^3. The helicon fringes and edge are more difficult to observe in aluminum than sodium, so that lower frequencies (30—300 kc/sec) were used to partially compensate for the greater ordinary (non-DSCR) attenuation in aluminum. For a given $\omega_c\tau$, the damping per wavelength is fixed, so that lower attenuation results when there are fewer wavelengths in the sample (lower frequency).

From the data, the number N of helicon half-wavelengths in the sample thickness, and thus the helicon wave number q, can be determined. The dispersion relation (1) is used for $B \gg B_E$, where the helicon behavior is local. The value of q for any lower B is then obtained by counting fringes down in field. The exact value of the Hall constant, $R_H = 1/ne$, to be used is a function of N. Discrepancies on the order of 5% between the expected theoretical value $1/ne$ and the experimentally determined value obtained from low-frequency-helicon experiments were at first conjectured to be due to many-body effects.[16] However, the theoretical work of Legendy[20] has since shown that the discrepancy is resolved when boundary effects are adequately taken into account. Our data substantiate this result. When N is large (≥ 10), boundary effects are not important, and we find we must not use the value of R_H determined from low-frequency-helicon experiments, but $1/ne$, the infinite-sample value, in order to obtain agreement with our data. On the other hand, for $N < 10$, boundary effects are expected to be important, and the low-frequency-helicon value for R_H does indeed fit our data in this region.

The plot of q^2 versus B^{-1} in Fig. 7(a) clearly demonstrates the nonlocal nature of the DSCR region for [100] Al. A similar plot for the [110] direction shown in Fig. 8 shows little deviation from the local behavior

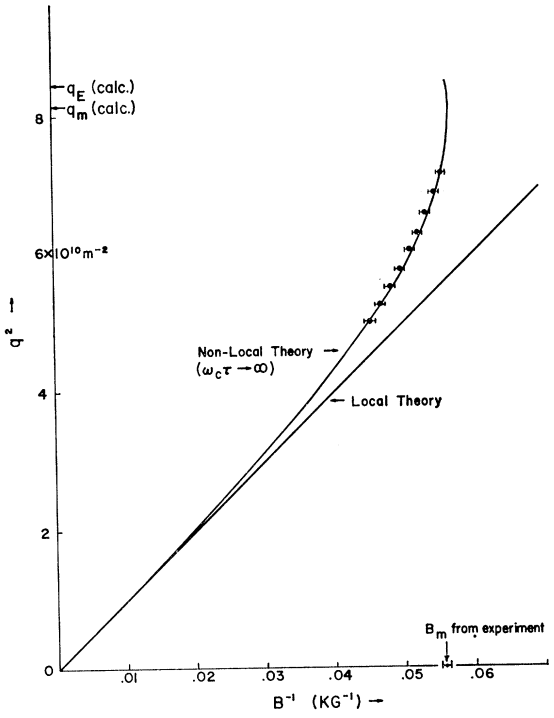

FIG. 4. Theoretical and experimental plot of the square of the helicon wave number q versus inverse magnetic field B^{-1}. The theoretical curves (solid lines) were calculated by a self-consistent method described in the text. They illustrate the local and nonlocal regions q_m (where the peak in surface resistance and zero helicon group velocity occur), and the Kjeldaas edge wave number q_E. The experimental points are for Na metal at 3 Mc/sec and 4.2°K. Sample thickness: 0.58 mm.

and, in particular, is not near the region with infinite slope. Theoretical calculations[10] have indicated that the infinite slope should be reached before the Kjeldaas edge is reached. Thus an experimental criterion to test if the measurements have approached the Kjeldaas edge

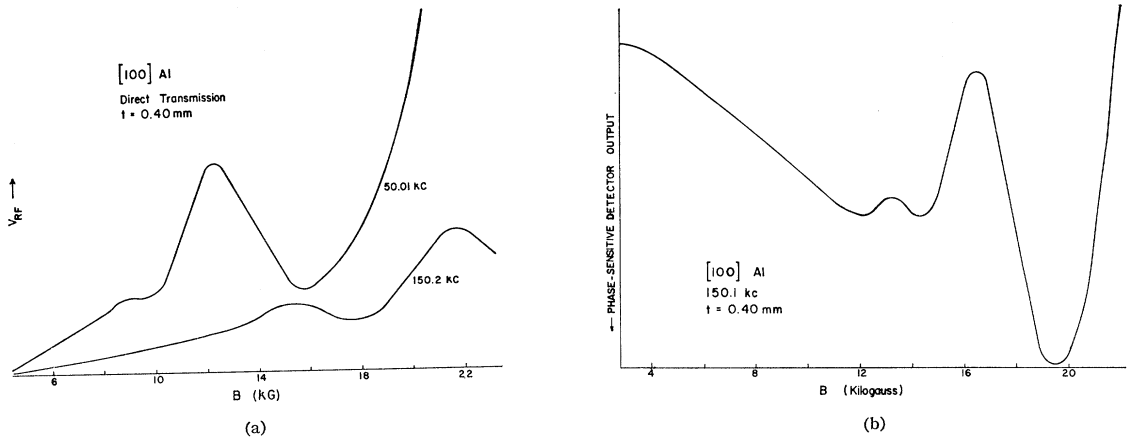

FIG. 5. (a) Tracing of direct transmission helicon fringes for single-crystal aluminum at 4.2°K. Sample normal and magnetic field are along [100]. Sample thickness: 0.40 mm. (b) Tracing of typical phase-sensitive detection curve. Same sample as in 5(a).

[20] C. R. Legendy, Phys. Rev. 135, A1713 (1964).

in addition to the one mentioned in Sec. III is that the q^2 versus B^{-1} plot should have a vertical slope. Since this does not occur for the [110] data, the disappearance of the helicon waves occurs before the edge.

Note that the [110] curves have a different low-field dependence than those of the [100] aluminum direct transmission curves.

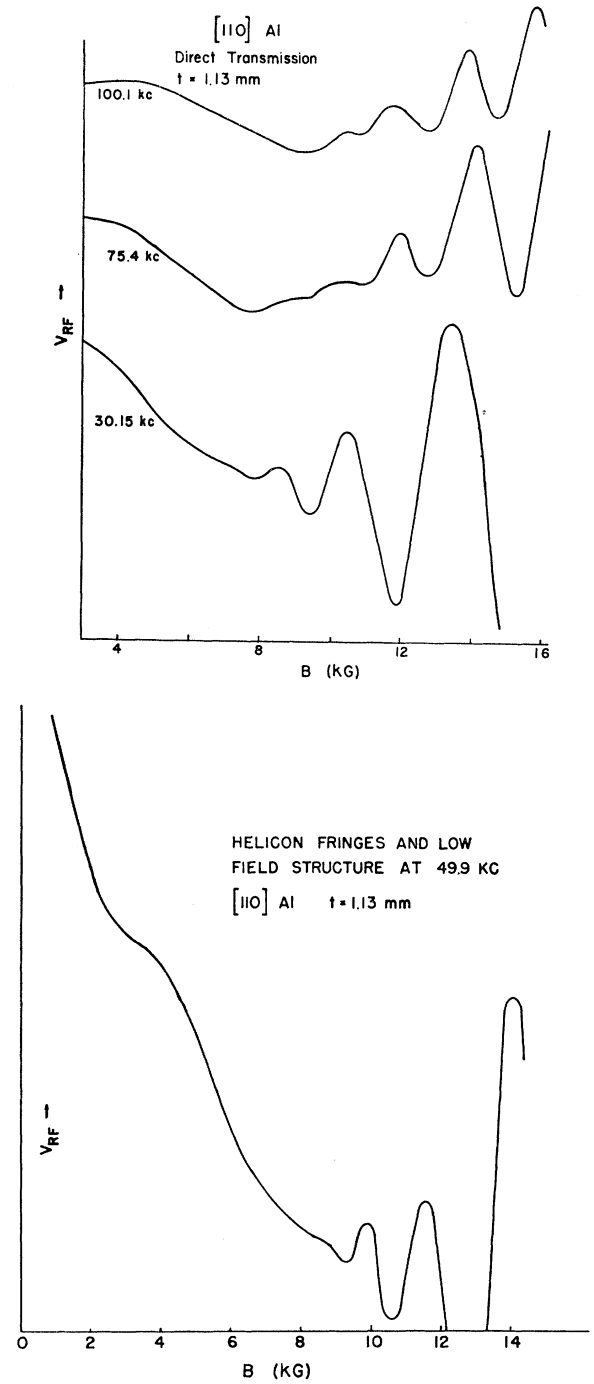

FIG. 6. (a) Tracing of typical helicon fringe data for [110] Al. Sample thickness: 1.13 mm. $T=4.2$°K. (b) Higher sensitivity showing low-field structure at 49.9 kc/sec. Same sample as in 6(a).

V. INTERPRETATION OF ALUMINUM RESULTS

A. [100] Aluminum

The [100] value of B_E is obtained from the maximum in the phase-sensitive detector output, below which (in field) the helicon waves are attenuated and the fringes disappear. This maximum corresponds to an inflection point in the direct transmission curve, because the derivative of the signal is obtained with a phase-sensitive detector of this type. The maximum in the [100] derivative curves is taken as the absorption edge for the following reasons:

(1) The [100] Al data have qualitatively the same edge character as Na where the edge field may be calculated theoretically due to its spherical Fermi surface. There we find that the measured derivative maximum occurs at the calculated edge to within experimental error.

(2) Even for the highest gain, the helicon fringes are observed down to, but never below, the derivative maximum.

(3) In the Appendix, we show that a behavior $B_E \propto \nu_E^{1/3}$, where ν is the helicon frequency, is expected for any general Fermi surface with closed orbits and infinite $\omega_c\tau$. For finite values of $\omega_c\tau$, B_E will be a function of $\omega_c\tau$, but the dependence is not strong.[10] Figure 7(b) shows an experimental plot of ν_E versus B_E for [100] Al. The agreement with the expected approximate $\nu_E^{1/3}$ dependence of B_E is good. On the other hand, plots of other structures (such as fringe maxima) near the edge do not show the correct dependence.

(4) The plot of q^2 versus B^{-1} in Fig. 7(a) shows an infinite slope at the field corresponding to the maximum in the [100] derivative curve. The DSCR absorption edge in the [100] direction is expected to occur at an elliptic limiting point in the second zone. As mentioned in Sec. II, theory indicates that for this case the infinite-slope field B_m is, within 1%, equal to the field at the absorption edge B_E. For these reasons, we take the [100] edge field as that of the derivative maximum where the helicon fringes die out. As will be discussed, there is good agreement between the theoretically expected curvature for [100] Al and the experimentally determined value.

The Fermi surface of aluminum is free-electron-like and has been investigated theoretically by several workers.[21,22] In the [100] direction, the second-zone surface obtained by Harrison has a spherical "cap." The sections in the third zone form a "monster." The sharp edges of the monster's arms become rounded when the lattice potential is adequately accounted for, yielding a curvature smaller than the free-electron value.

In contrast, the [100] "cap" of the second zone is expected to have a nearly free-electron curvature, since

[21] W. A. Harrison, Phys. Rev. 118, 1182 (1960).
[22] N. W. Ashcroft, Phil. Mag. 8, 2055 (1963).

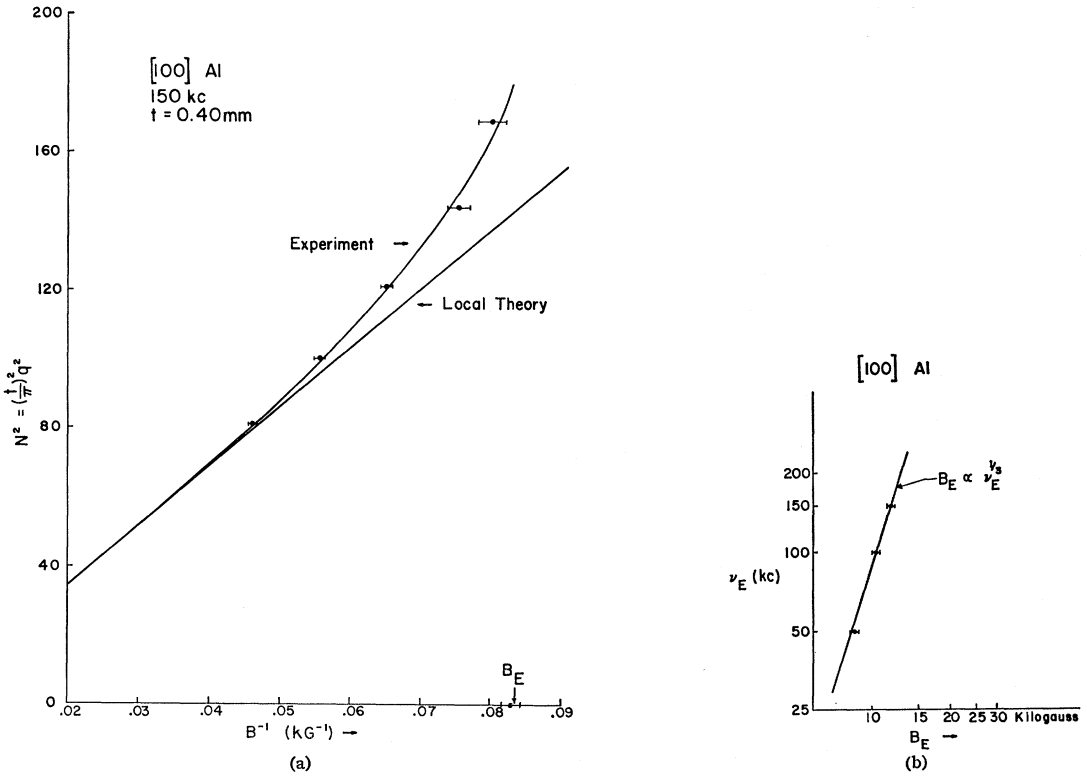

FIG. 7. (a) Plot of the square of the number of half-wavelengths N in the sample thickness versus B^{-1}. N is proportional to the helicon wave number q. The helicon frequency is 150 kc/sec and the [100] Al sample is 0.40 mm thick. (b) Plot of edge frequency versus edge field for [100] Al. The solid line is drawn through the data points and corresponds to a $B_E \propto \nu_E^{1/3}$ dependence.

the Brillouin-zone boundaries are relatively far away, leaving the cap practically undistorted. Recall that only the absorption edge with the largest curvature will be seen in helicon DSCR studies because the helicons are so heavily attenuated inside an absorption edge. Thus, the [100] absorption edge is expected to occur at the elliptic limiting point of the second zone "cap," and to have a curvature close to the free-electron value. Since the third-zone curvature is smaller, its absorption edge will lie lower in field than that of the second zone, and is not expected to be seen.

We define a normalized curvature parameter

$$\mathfrak{R} = |\partial A/\partial k_B|_{max}/2\pi k_F, \tag{9}$$

which for an elliptic limiting point becomes

$$\mathfrak{R} = (\rho_1\rho_2)^{1/2}/k_F. \tag{10}$$

For a spherical surface, $\rho_1 = \rho_2 = k_F$, and $\mathfrak{R}$ has the value unity.

The experimental data yield the following values of $\mathfrak{R}$ for the [100] direction of aluminum:

Helicon frequency	$\mathfrak{R}$
50 kc/sec	1.01±0.05
100 kc/sec	1.00±0.06
150 kc/sec	0.97±0.05

This yields a result of

$$\mathfrak{R} = 0.99 \pm 0.03 \tag{11}$$

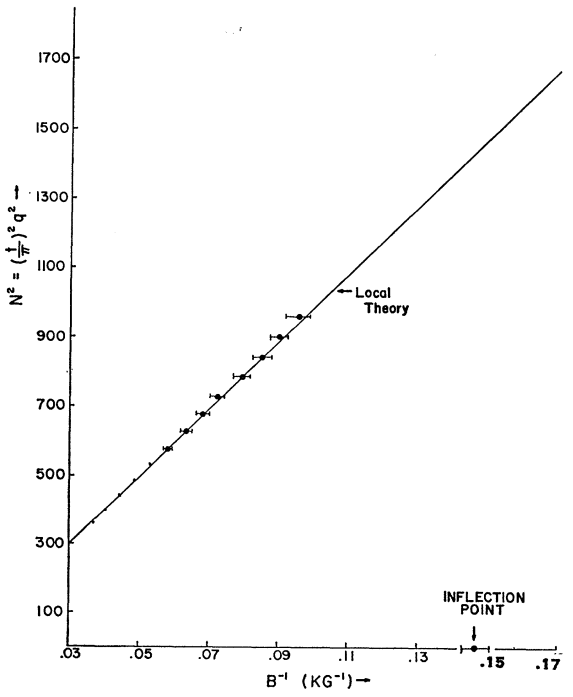

FIG. 8. Plot of the square of the number of half-wavelengths N in the [110] sample thickness versus B^{-1}. N is proportional to the helicon wave number q. The helicon frequency is 100 kc/sec and the [110] sample thickness is 1.13 mm.

for the [100] direction in aluminum, in good agreement with the expected value of unity.

B. [110] Aluminum

The [110] Al data have a different low field behavior than that of the [100] Al and the polycrystalline-Na data.

The following characteristics, consistent throughout the data, may be enumerated for the [110] direction:

(1) With highest gain, the helicon fringes are not seen to disappear at an inflection point, although an inflection point is found at lower fields.

(2) The structure in the vicinity of the inflection point varies in field approximately as the cube root of the helicon frequency. This is the same behavior as that observed for [100] Al and polycrystalline Na, and is the expected behavior for an absorption edge. (See the Appendix.)

(3) The helicon behavior is found to be still essentially local down to the field for which the fringes disappear, in contrast to the [100] data (see Fig. 8).

Especially from (3), we see that the helicon waves disappear well before the absorption edge is reached in [110] as contrasted to the [100] direction. In order to understand this difference with respect to crystallographic orientation, we now investigate the properties of the aluminum Fermi surface when the magnetic field lies along [110]. With the field along [110], the limiting

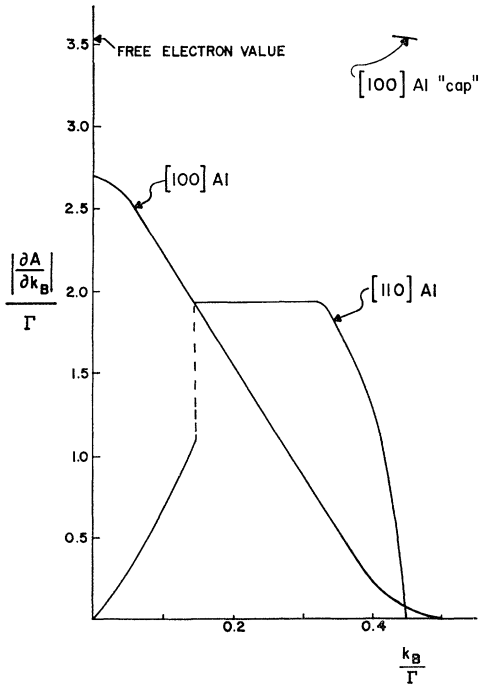

FIG. 9. Plot of $|\partial A/\partial k_B|$ versus k_B for [100] and [110] Al. A is the area enclosed by a cyclotron orbit and k_B is the electronic wave number along the field. Γ is the [100] diameter of the Brillouin zone.

point of the second zone is a saddle-shaped surface. A saddle-shaped surface does not have a point-limiting orbit, but rather a figure-eight orbit of low $\partial A/\partial k_B$, so that the first absorption edge will occur for other parts of the Fermi surface.

Other second-zone orbits which are likely to have an observable absorption edge are those for which $\partial A/\partial k_B$ has a maximum value. Jones[23] has given plots of the area A enclosed by a cyclotron orbit as a function of electronic momentum along the field, for the field lying along [100] and [110] in Al. We have numerically differentiated these curves to obtain the $\partial A/\partial k_B$ curves shown in Fig. 9.

For the field along [100], the greatest value of $\partial A/\partial k_B$ for the second zone, aside from the "cap," is about 77% of the free-electron curvature, $2\pi k_F$. Since only the absorption edge with the greatest curvature will be seen by the helicon DSCR method, this lower curvature will not be observed. The observed edge occurs on the "cap" as discussed above.

In contrast, the second zone along [110] has no "cap," but a saddle-point of low $\partial A/\partial k_B$. Hence, any absorption edge due to second-zone carriers must come from other orbits. Figure 9 reveals the unsuspected result that a large fraction ($\sim$50%) of the orbits on the Fermi surface have the same value of $\partial A/\partial k_B$, and that this value is higher than that for any of the other second-zone orbits. The value of the curvature parameter for these orbits is calculated from the derivative curve to be

$$\mathcal{R}=0.52\pm0.02. \tag{12}$$

An absorption edge will occur because of these electrons on finite orbits, unless a higher curvature exists on the third-zone surface. Even if (12) is slightly lower than the largest value found, it would not be surprising to see vestiges of the orbits reflected in the sample surface impedance, since such a large fraction of the carriers come into cyclotron resonance simultaneously.

We must next ask whether a curvature greater than (12) exists in the third zone. The largest curvature will occur on an arm of the third-zone surface, and has the free-electron value in the SOPW model[21] of Harrison. However, when the lattice potential is included, the curvature is reduced. The minimum radius of curvature ρ_2 lies in a plane perpendicular to the intersection of the two Brillouin-zone boundaries that cut out the third-zone arm, and is strongly affected by the effects of the lattice potential. The maximum radius of curvature of the arm, ρ_1, on the other hand, is not affected at all by the two aforementioned Brillouin zone boundaries, and only weakly affected by other boundaries farther off in k space. To first approximation it will retain its free-electron value, k_F.

Ashcroft[22] has utilized the latest de Haas–van Alphen data to calculate the principle cross section of the third-

[23] B. K. Jones, Phil. Mag. 9, 217 (1964).

zone arm for aluminum. We are indebted to Dr. Ashcroft for very generously supplying us with more extensive data from his machine calculations on aluminum. From this data we have calculated ρ_2 and find:

$$\rho_2 = (0.31 \pm 0.01) k_F. \tag{13}$$

Taking $\rho_1 \cong k_F$ to first order, the curvature parameter for the elliptic limiting point on the third-zone arm is found to be

$$\mathcal{R} \cong 0.55. \tag{14}$$

Thus, comparing (12) and (14), we find that the maximum value of the curvature parameters for the second and third zones is practically the same. The absorption edges for the finite second-zone orbits and the elliptic limiting point third-zone orbit are therefore expected to occur almost simultaneously. It is just this property of the aluminum Fermi surface with the field along [110] that we envoke as an explanation of the observed differences compared to the [100] direction. Calculations show that the real part of the effective conductivity for helicons for a point-orbit edge rises with finite slope from zero at the edge, since the first electrons contributing to the absorption are the small number on a "point" orbit. However, for a finite-orbit edge, a much larger number of electrons, on a finite orbit, first contribute to the absorption edge, and the real part of the conductivity suffers a discontinuous jump from zero to a large value as the absorption edge is reached.[4,24] The effect of finite $\omega_c\tau$ is to smear out the absorption edge. It will be seen that the magnitude of the attenuation near the edge ($B \gtrsim B_E$) due to finite $\omega_c\tau$, will be much larger for the finite-orbit edge than for the point-orbit-edge case. For a finite-orbit edge such as in [110] Al, where such a large fraction of the carriers come into resonance simultaneously, the effect will be even more pronounced. This is in agreement with the observed differences in the Al data: Along [110], where the finite-orbit edge is expected to occur, the fringes are not seen down to an "edge," but disappear as they enter the nonlocal region. The [100] direction, with an elliptic limiting-point-orbit edge, allows fringe detection down to the edge. We conclude that this difference is a manifestation of the different characteristics of finite- and point-orbit edges.

For low values of $\omega_c\tau$, it is difficult to accurately determine B_m because the experimental coil-sample configuration does not reflect either the purely resistive or purely reactive change in the sample surface impedance, but some combination of both. For low $\omega_c\tau$, where the structure in R and X is much less pronounced, care should be exercised (as discussed Sec. II) in assigning the exact location of B_m within the observed structure. The best method for low $\omega_c\tau$ is that used here in the [100] Al case: observation of helicon fringes down to, and their disappearance at, a structure (in this case an inflection point).

Because of the above discussion of the effects of low $\omega_c\tau$ on the edge structure ($\omega_c\tau \sim 10$ here), together with the fact that the [110] fringes damp out before the edge, we do not attempt a precise edge and curvature determination for [110]. We propose that the inflection structure is a reflection in the rf coil impedance of the sample surface impedance changes due to the DSCR edge phenomena. As discussed in Sec. II, this structure occurs at B_m, not B_E. For a finite orbit edge, the difference may be considerable, so that we do not assign B_E to the inflection point in the [110] data, as was the case for [100], because of the strong contrast in Fermi-surface topology expected between [110] and [100]. Instead we can only assign B_m to the *vicinity* of the inflection structure.

While it is not possible to obtain the exact value of the edge from our [110] data, it is possible to estimate the order of magnitude of the [110] curvature. If the edge is taken at the inflection point and the value of q_E estimated by extrapolation from the local regime, the [110] data for 30 to 300 kc/sec yield a value

$$\mathcal{R} \sim 0.56 \tag{15}$$

in surprisingly good agreement with the expected values, (12) and (14). The closeness of the agreement is certainly fortuitous, considering the approximations involved.

VI. CONCLUSIONS

The properties of the aluminum Fermi surface were studied with the magnetic field along [100] and [110]. For [100], it was shown that the expected edge should occur on a "spherical cap" with Gaussian curvature close to the free-electron value. The experimental value obtained was 0.99 ± 0.03 of the free-electron radius of curvature, in good agreement with theory.

For [110] Al, we have shown that an elliptic-limiting-point orbit edge on an arm of the third-zone Fermi-surface "monster," and a finite-orbit edge due to finite orbits involving a large fraction of the electrons on the second-zone surface, are expected to occur almost simultaneously. For this reason and the fact that $\omega_c\tau$ is low (~ 10) for these edges, the [110] data are more complicated and interpretation is difficult. We have not attempted a precise interpretation for [110], beyond showing that an estimate of the [110] curvature is in surprisingly good agreement with the expected edge values. Because of the uncertainties involved with a finite-orbit-edge case and low $\omega_c\tau$, a more precise interpretation is neither warranted nor justifiable.

If material with sufficiently high $\omega_c\tau$, on the order of 100 or more, can be obtained, the helicon-interference-fringe method should allow measurement of both q_m and q_E, the latter being directly related to the Fermi-surface curvature. If only q_m or B_m is obtained, as in the

[24] G. L. Kotkin, Zh. Eksperim. i Teor. Fiz. 41, 281 (1961) [English transl.: Soviet Phys.—JETP 14, 201 (1962)].

surface impedance method, caution must be exercised in interpreting the data, since the difference between these quantities and those directly related to the Fermi surface curvature, q_E and B_E, is not expected to be insignificant when finite-orbit edges are involved.

Although the helicon DSCR method can yield valuable Fermi-surface information, the technique is not very useful when high magnetoresistance, low $\omega_c\tau$, and complicated Fermi surface topology are present. Thus, it is not likely that it will replace the more proven, general techniques such as the de Haas–van Alphen and magnetoacoustic methods for Fermi surface investigations, though it could supplement these techniques.

ACKNOWLEDGMENTS

It is a pleasure to acknowledge stimulating discussions with Professor J. F. Koch and Dr. J. C. McGroddy. The technical assistance of O. H. McKim, Eric Katz, J. R. Maldonado, and T. K. Wagner is appreciated.

One of us (J. L. S.) wishes to thank the National Science Foundation for support in the form of a Cooperative Predoctoral Fellowship during the course of this investigation.

APPENDIX

Proof that the absorption-edge field is proportional to the cube root of the edge frequency in the limit of $\omega_c\tau\to\infty$.

From Maxwell's equations, the general helicon dispersion relation neglecting the displacement current is

$$q^2=\omega\mu_0 i\sigma(q), \tag{16}$$

where $\sigma(q)$ is the conductivity appropriate for helicons. In the DSCR region, σ is in general nonlocal in nature and wave-number–dependent.

Because the condition $\omega\ll\omega_c$ is realized in experiment, the condition for DSCR helicon absorption is, from (2)

$$\omega_c=q\bar{v}_B. \tag{17}$$

At the absorption edge, $\bar{v}_B=(\bar{v}_B)_{\max}=v_M$. With the definition $\omega_c=eB/m^*$, as $q\to q_E$ the edge condition becomes

$$(eB_E/m^*v_M)^2=-\omega_E\mu_0\,\mathrm{Im}\sigma(q_E). \tag{18}$$

The dependence of $\sigma(q_E)$ on B may be found by extending the impulsive method of Pippard[25] to include nonlocal effects. We calculate the current component dJ_i set up by an impulsive electric field $E_j=E_{j0}e^{i(qz-\omega t)}dt$ in the presence of a steady field B along the z axis. A factor $e^{t/\bar{\tau}}$ is included to account for electron-lattice scattering at times $t<0$, where $\omega_c\bar{\tau}\gg1$ so that $\bar{\tau}$ is the average scattering time around a given orbit.

For a general Fermi surface, the motion of a group of carriers on an orbit defined by the intersection of the Fermi surface and the plane $k_z=$constant may be represented by a Fourier series, so that the current from the whole Fermi surface (FS) due to E_j is

$$dJ_i=\int_{\mathrm{FS}}dk_z\sum_{n=-\infty}^{\infty}A_{ij}^{(n)}e^{-in\omega_c t}E_{j0}e^{i(qz-\omega t)+t/\bar{\tau}}dt. \tag{19}$$

Note that open orbits, by their very nature, do not have a cyclotron period and thus cannot generally be represented by (19). We thus restrict ourselves to Fermi surfaces having no open orbits for the direction of B chosen.

Taking the nonlocal behavior into explicit account by integrating over time from $-\infty$ to 0, we find

$$J_i=\sum_n\int_{\mathrm{FS}}dk_z\frac{A_{ij}^{(n)}(k_z)E_{j0}}{i(q\bar{v}_z-\omega-n\omega_c)-1/\bar{\tau}}, \tag{20}$$

where we have taken $z=\bar{v}_z t$.

In general, ω_c is a function of k_z:

$$\omega_c(k_z)=eB/m^*(k_z)=g(k_z)B. \tag{21}$$

With the definition $\sigma_{ij}=J_i/E_{j0}$ at $t=0$, plus the fact that $\omega\ll\omega_c$ for helicons in metals,

$$\sigma_{ij}(\omega=0,q)=-\frac{i}{B}\sum_n\int_{\mathrm{FS}}dk_z\times\frac{A_{ij}^{(n)}(k_z)g^{-1}(k_z)}{[(q/B)(\bar{v}_z(k_z)/g(k_z))-n]+i/\omega_c\bar{\tau}}. \tag{22}$$

Thus,

$$\mathrm{Im}\sigma_{ij}(0,q)\big|_{\omega_c\tau\to\infty}=-(1/B)G(\zeta), \tag{23}$$

where

$$\zeta=q/B.$$

The diagonal terms of σ are required by symmetry to be even functions of B. As $\omega_c\tau\to\infty$ the off-diagonal terms dominate since the diagonal terms are at least of order B^{-2}. At the absorption edge, Eq. (3) shows that ζ takes on the value

$$\zeta_E=(2\pi e/\hbar)(|\partial A/\partial k_B|_{\max})^{-1}, \tag{24}$$

which is dependent only on the topology of the Fermi surface. Thus,

$$\mathrm{Im}\sigma(0,q_E)=-(1/B_E)G(\zeta_E). \tag{25}$$

This result, combined with (18), yields

$$B_E\propto\omega_E^{1/3}, \tag{26}$$

which was to be proved. It is good to reiterate the conditions upon which (26) is contingent:

(1) Any general Fermi surface, so long as there are no open orbits for the direction of B chosen.

(2) $\omega_c\tau\to\infty$.

[25] A. B. Pippard, Rept. Progr. Phys. **23**, 176 (1960).